Eur. Phys. J. C (2018) 78:60
https://doi.org/10.1140/epjc/s10052-018-5549-y

THE EUROPEAN PHYSICAL JOURNAL C

Regular Article - Theoretical Physics

Light stops and fine-tuning in MSSM

Ali Çiçi[a], **Zerrin Kırca**[b], **Cem Salih Ün**[c]

Department of Physics, Uludağ University, TR16059 Bursa, Turkey

Received: 4 August 2017 / Accepted: 13 January 2018 / Published online: 23 January 2018

Abstract We discuss the fine-tuning issue within the MSSM framework. Following the idea that the fine-tuning can measure effects of some missing mechanism, we impose non-universal gaugino masses at the GUT scale, and explore the low scale implications. We realize that the fine-tuning parametrized with Δ_{EW} can be as low as zero. We consider the stop mass with a special importance and focus on the mass scales as $m_{\tilde{t}} \leq 700$ GeV, which are excluded by the current experiments when the stop decays into a neutralino along with a top quark or a chargino along with a bottom quark. We find that the stop mass can be as low as about 250 GeV with $\Delta_{EW} \sim 50$. We find that the solutions in this region can be exluded only up to 60% when stop decays into a neutralino-top quark, and 50% when it decays into a chargino-b quark. Setting 65% CL to be potential exclusion and 95% to be pure exclusion limit such solutions will be tested in near future experiments, which are conducted with higher luminosity. In addition to stop, the region with low fine-tuning and light stops predicts masses for the other supersymmetric particles such as $m_{\tilde{b}} \gtrsim 700$ GeV, $m_{\tilde{\tau}} \gtrsim 1$ TeV, $m_{\tilde{\chi}_1^\pm} \gtrsim 120$ GeV. The details for the mass scales and decay rates are also provided by tables of benchmark points.

1 Introduction

The Standard Model (SM) of the elementary particles is one of the most successful theories in physics, which has been being tested and confirmed by the strictest experiments for decades. On the other hand, despite the Higgs boson discovery by the ATLAS [1] and CMS [2] experiments, the SM can only be an effective theory, since it is problematic in stabilizing the Higgs boson mass against the quadratic divergent radiative corrections. Supersymmetry, one of the forefront candidates for physics beyond the SM, can resolve this severe problem by adding superpartners for the SM particles in minimal supersymmetric version of the SM (MSSM). In addition, the tree gauge couplings of the SM can nicely unify at a scale ($\sim 2 \times 10^{16}$ GeV), and hence one can build supersymmetric grand unified theories (GUT) to investigate physics at much higher energy scales. Since the Higgs boson mass is free from the quadratic divergences in the MSSM framework, such GUT models can be linked to the low energy scales through the MSSM renormalization group equations (RGEs), which make possible to explore their low scale implications at the current experiments.

Even though the MSSM predictions can be consistent with the current Higgs boson measurements, they have a strong impact in shaping the fundamental parameter space of MSSM. First of all, the MSSM predicts $m_h \lesssim M_Z$ for the Higgs boson mass at tree level. This inconsistency requires large radiative corrections to be consistent with $m_h \sim 125$ GeV. Since the first two family matter particles have negligible couplings to the Higgs boson, the third family particles play a crucial role in radiative contributions to the Higgs boson mass. Moreover, the sbottom and stau, superpartners of bottom quarks and tau lepton respectively, can easily destabilize the Higgs potential [3]; thus the stability condition on the Higgs potential allows only minor contributions from these sparticles. On the other hand, contributions from the stop, superpartner of top quark, has more freedom without disturbing the Higgs potential stability. After all, the stop sector forms the main source of large radiative corrections to the Higgs boson mass. In order to realize the Higgs boson of mass about 125 GeV, one needs either multi-TeV stop mass, or relatively large soft supersymmetry breaking (SSB) trilinear A_t-term [4,5].

Besides the Higgs boson impact, the stop sector can be constrained further by the null results from the direct searches of sparticles at the Large Hadron Collider (LHC). The exclusion on the stop mass depends on the stop's decay channel. If stop is kinematically allowed only to decay into a charm

[a] e-mail: 501507007@ogr.uludag.edu.tr
[b] e-mail: zkirca@uludag.edu.tr
[c] e-mail: cemsalihun@uludag.edu.tr

quark and neutralino, then the stop mass bound can be as low as about 230 GeV [6]. The constraint becomes much more severe when the stop can decay into a bottom quark, a W-boson and a neutralino. In this case the solutions with stop mass lighter than 650 GeV are excluded [7]. The strictest channel is the one in which the stop decays into a top quark and a neutralino. This channel bounds the stop mass from below at about 750 GeV [8].

In this context, the current results and constraints yield heavy mass spectrum for the SUSY particles, and it brings us back to the naturalness problem. If one characterizes the natural region in SUSY models with $m_{\tilde{t}_1}, m_{\tilde{t}_2}, m_{\tilde{b}_1} \lesssim 500$ GeV [9–12], it is clearly not possible to fit MSSM consistently in the natural region. Even if the lightest stop mass can be realized as $m_{\tilde{t}_1} \lesssim 500$ GeV, the heaviest stop mass eigenstate should be $m_{\tilde{t}_2} \gtrsim 1$ TeV to yield a 125 GeV Higgs boson solution [13]. Such a large splitting between two mass eigenstates of stop indicates a large mixing between the flavor eigenstates, which is proportional to A_t. Similarly, sbottom is also found heavier than about 1 TeV.

One proceeds in the naturalness discussion by considering the required fine-tuning in SUSY models, which is discussed in more details in the next section. In this paper, we consider the MSSM framework with non-universal gauginos ($M_1 \neq M_2 \neq M_3$) and explore the regions with acceptable fine-tuning. Non-universal SSB mass terms for the gauginos can be realized when the gaugino masses are generated with F-terms, which are not singlet under the GUT gauge group [14–18]. It has been pointed out in [19] that if the bilinear Higgs mixing is set to be negative ($\mu < 0$), then the results exhibit more tendency to yield much lower fine-tuning and even light stop solutions, even as light as top quark. However, in the case with $\mu < 0$, the SUSY particles destructively contribute to muon anomalous magnetic moment (muon $g-2$); thus the results for muon $g-2$ are worse than the SM predictions. This drawback can be avoided by setting also $M_1, M_2 < 0$, where M_1 and M_2 are the SSB gaugino masses associated with $U(1)_Y$ and $SU(2)_L$ respectively.

After the physical implications within the fundamental parameters space are investigated, we focus on the solutions with the stop mass lighter than 700 GeV, and discuss the LHC exclusion for these light stop solutions over some benchmark points. The outline of our paper is the following: We first define the parameter to determine the required fine-tuning at the low scale in Sect. 2. We also discuss the implications and restrictions from the fine-tuning constraint in this section. Section 3 describes the data generation and analyses along with the fundamental parameter space and the experimental constraints employed in our analyzes. Then, we discuss our results for the fine-tuning with highlighting the light stop solutions ($m_{\tilde{t}_1} \lesssim 700$ GeV) in Sect. 4. After discussing the impact of the fine-tuning and light stop solutions, we also present the mass spectrum for the other sparticles in Sect. 5. In Sect. 6 we analyze if the LHC can detect such light stop solutions over some benchmark points. Finally we conclude in Sect. 7.

2 Low scale fine-tuning measurement

Compared to the SM, the Higgs sector is more complicated in the MSSM, since there are two Higgs doublets, which both develop non zero vacuum expectation values (VEVs). Also, it has been shown a long time ago that the SUSY has to be broken to realize the correct EW breaking scale (~ 100 GeV), since the minimization of the Higgs potential requires $m_{H_u} \neq m_{H_d}$ [20]. As discussed in the previous section, the fundamental parameter space of MSSM needs to be fine-tuned, and it can be analyzed by considering the $Z-$boson mass with the following equation

$$\frac{1}{2}M_Z^2 = -\mu^2 + \frac{(m_{H_d}^2 + \Sigma_d) - (m_{H_u}^2 + \Sigma_u)\tan^2\beta}{\tan^2\beta - 1}, \quad (1)$$

where μ is the bilinear mixing term, $m_{H_{d,u}}$ are the SSB mass terms for the MSSM Higgs fields. $\Sigma_{d,u}$ denote the radiative contributions to $m_{H_{d,u}}$ respectively. $\tan\beta$ is the ratio of the vacuum expectation values (VEVs) as $\tan\beta = v_u/v_d$. The left hand side of Eq. (1) is precisely determined by the experiments, while the right hand side is involved with the fundamental parameters of MSSM, whose values can lie in a wide range. Thence, there needs to be significant cancellations among the parameters in the right hand side to yield consistent M_Z. Since the terms with m_{H_d} (and Σ_d) are suppressed by $\tan\beta$, the cancellations happen mainly among the terms with μ and m_{H_u}, and the correct EW breaking scale requires $\mu \approx m_{H_u}$ over most of the fundamental parameter space. The required amount of fine-tuning can be quantified with Δ_{EW}, which is defined based on Eq. (1) as

$$\Delta_{EW} \equiv \mathrm{Max}(C_i)/(M_Z^2/2),$$
$$\text{where} \quad C_i = \begin{cases} C_{H_d} = |\, m_{H_d}^2/(\tan^2\beta - 1)\,| \\ C_{H_u} = |\, m_{H_u}^2 \tan^2\beta/(\tan^2\beta - 1)\,| \\ C_\mu = \ |\, -\mu^2\,|, \end{cases} \quad (2)$$

here we have assumed that the radiative corrections $\Sigma_{d,u}$ are included in $m_{H_{d,u}}$. In contrast to characterizing the natural region, the amount of fine-tuning does not depend on the sparticle masses directly. However, the sparticle spectrum and mixings among them are still important, since they take part in radiative corrections to $m_{H_{d,u}}$.

If it is possible to realize low μ^2 values over the fundamental parameter space, the fine-tuning can be found in an acceptable range regardless of the sparticle mass spectrum.

However, the effects from the sparticle masses are encoded in the radiative corrections. Σ_d is evolved with the sbottom and stau masses, which contribute to m_{H_d} at the loop level. Since this term is suppressed by $\tan\beta$, the effects from the sbottom and stau masses in the fine-tuning are minor. On the other hand, Σ_u, which arises from the stop sector, does not exhibit a suppression by $\tan\beta$. Large stop masses or large mixings between left and right handed stops can significantly contribute to the radiative corrections which result in large m_{H_u}, and thus large μ-term. Considering the severe experimental exclusion limits on stops, discussed in the previous section, it is obvious that the parameter space, allowed by the experiments, needs to be largely fine-tuned. Even if one restricts the lightest stop masses to be at a few hundred GeV, then a large mixing between stops is required by the Higgs boson mass. Such a large mixing results in very large radiative corrections, and hence, raises the required fine-tuning significantly [19]. This discussion can be concluded that the SUSY models need large fine-tuning when the sparticle and the gaugino masses are set universal at the GUT scale.

If one relaxes the exclusion limits from the LHC, mentioned above, and allows the solutions with light stop, the required fine-tuning can potentially be improved at the low scale. However, the requirement to yield the Higgs boson of mass about 125 GeV also puts a severe constraint on the stop masses as discussed in the previous section. The Higgs boson mass within the MSSM can be written as

$$m_h \approx M_Z \cos\beta + \frac{3m_t^4}{4\pi^2 v^2}\left(\log\frac{M_S^2}{m_t^2} + \frac{X_t}{M_S^2} - \frac{X_t^4}{12M_S^4}\right) - \frac{y_b^4\mu^4 v^2}{16\pi^2 M_S^4} \tag{3}$$

where m_t is the top quark mass, while $M_S \equiv \sqrt{m_{\tilde{t}_L} m_{\tilde{t}_R}}$ is the average stop mass. M_S is also the energy scale at which the supersymmetric particles decouple from the SM. The mixing in the stop sector is encoded in X_t as $X_t = A_t - \mu\cot\beta$, where A_t stands for this mixing. The first term in Eq. (3) is the tree-level mass of the Higgs, and it can only be about 90 GeV at most. Thus, it needs significant loop corrections to realize the Higgs boson of mass about 125 GeV. Such large corrections can be obtained with a large mass splitting between the stop and top quarks ($M_S \gg m_t$). Another way to raise the loop corrections is to implement large mixing in the stop sector. We should note that here $A_t \lesssim 3M_S$ should be satisfied not to break color and/or charge conservation at minima of the scalar potential [21]. Hence, in the case of large mixing, sparticles cannot be lighter than certain mass scales.

The last term in Eq. (3) with the b-quark Yukawa coupling (y_b) and the VEV of the Higgs boson (v) represents loop contributions from the bottom sector, and it is rather significant when $\tan\beta$ is large. Note that this contribution reduces the Higgs boson mass, and the stop sector should contribute more to compensate its diminishing effect, while the Higgs boson mass can be realized as about 125 GeV. Such a compensation can be achieved with a large A_t term. In this context, this term can also have significant impact on the fine-tuning issue indirectly through the stop sector. In addition, the Higgs boson coupling to the bottom sector can easily destabilize the Higgs potential, and hence stabilization condition restricts $\mu\tan\beta$ such that it allows only minor contributions from the bottom sector [3].

Consequently, the only dominant source for large loop corrections to the Higgs boson mass is the stop sector, which requires the stop to be heavier even if the mixing in this sector is large. This situation can be drastically different if MSSM is extended with new particles and/or new symmetries [22–27] which contribute to the Higgs boson mass as significantly as the stop. In this context, the minimal supersymmetric models may not cover the full picture of physics. The mechanisms, which are not included in the minimal models, can affect the low scale phenomenology. In this sense, the fine-tuning requirement can emerge because of some missing mechanisms, and its amount can be interpreted as the effectiveness of these missing mechanisms, and also indicates the amount of deviation from the minimality. The effects from missing mechanisms can be analyzed also within the MSSM framework by implementing non-universalities in gaugino and scalar sectors [28–31]

In our work, we analyze the effects of possible missing mechanisms within the MSSM framework by imposing non-universality in the gaugino sector. While we focus on the regions with low fine-tuning, we also highlight the stop masses less than 700 GeV, and discuss if such solutions can still survive under the severe experimental constraints.

3 Scanning procedure and experimental constraints

We have employed SPheno 3.3.8 package [32,33] obtained with SARAH 4.5.8 [34,35]. In this package, the weak scale values of the gauge and Yukawa couplings present in MSSM are evolved to the unification scale $M_{\rm GUT}$ via the renormalization group equations (RGEs). $M_{\rm GUT}$ is determined by the requirement of the gauge coupling unification through their RGE evolutions. Note that we do not strictly enforce the unification condition $g_1 = g_2 = g_3$ at $M_{\rm GUT}$ since a few percent deviation from the unification can be assigned to unknown GUT-scale threshold corrections [36,37]. With the boundary conditions given at $M_{\rm GUT}$, all the SSB parameters along with the gauge and Yukawa couplings are evolved back to the weak scale.

We have performed random scans over the following parameter space

$$\begin{aligned} 0 \leq \quad & m_0 \quad \leq 10 \text{ TeV} \\ -10 \leq \quad & M_1 \quad \leq 0 \text{ TeV} \\ -10 \leq \quad & M_2 \quad \leq 0 \text{ TeV} \\ 0 \leq \quad & M_3 \quad \leq 10 \text{ TeV} \\ -3 \leq \quad & A_0/m_0 \quad \leq 3 \\ 2 \leq \quad & \tan\beta \quad \leq 60 \end{aligned} \tag{4}$$

$$\mu < 0, \quad m_t = 173.3 \text{ GeV}$$

where m_0 is the universal SSB mass term for the matter scalars and Higgs fields. M_3, M_2 and M_1 are SSB mass terms for the gauginos associated with the SU(3), SU(2) and U(1) symmetry groups respectively. A_0 is SSB trilinear coupling, and $\tan\beta$ is ratio of VEVs of the MSSM Higgs doublets. In the constrained MSSM (CMSSM) with non-universal gauginos all matter scalars have the same mass and gaugino masses can be chosen different from each other at the GUT scale. The radiative EW breaking (REWSB) condition determines the value of μ-term but not its sign; thus, its sign is one of the free parameters, and we set it negative in our scans. In addition, we have used central value of top quark mass as $m_t = 173.3$ GeV [38]. Note that the sparticle spectrum is not too sensitive to one or two sigma variation in the top quark mass [39], but it can shift the Higgs boson mass by 1–2 GeV [40,41].

The REWSB condition provides a strict theoretical constraint [42–46] over the fundamental parameter space given in Eq. (4). Another important constraint comes from the relic abundance of charged supersymmetric particles [47]. This constraint excludes the regions which yield charged particles such as stop and stau being the lightest supersymmetric particle (LSP). In this context, we accept only the solutions which satisfy the REWSB condition and yield neutralino LSP. When one requires the solutions to yield one of the neutralinos to be LSP, it is also suitable that the LSP can be promoted as a candidate for dark matter. In this case, the relic abundance of LSP should also be consistent with the current results from the WMAP [48] and Planck [49] satellites. However, even if a solution does not satisfy the dark matter observations, it can still survive in conjunction with other form(s) of the dark matter formation [50,51]. In this case, the lightest neutralino may not be related to the DM phenomenology. On the other hand, the collider analyses performed by the CMS and ATLAS experiments assume the lightest neutralino to be LSP. In this context, we will allow only the solutions which are compatible with the LSP neutralino condition to compare our results one to one with the CMS and ATLAS analyses [52], while we do not require the solutions to satisfy the DM constraints.

In scanning the parameter space we use our interface, which employs Metropolis-Hasting algorithm described in [53,54]. After collecting the data, we successively apply the mass bounds on all sparticles [55] and the Higgs boson [56] and the constraints from the rare B-decays ($B_s \to \mu^+\mu^-$ [57], $B_s \to X_s\gamma$ [58] and $B_u \to \tau\nu_\tau$ [59]). The experimental constraints can be listed as follows:

$$\begin{aligned} & 123 \leq m_h \leq 127 \text{ GeV} \\ & m_{\tilde{g}} \geq 1000 \text{ GeV} \\ & 0.8 \times 10^{-9} \leq BR(B_s \to \mu^+\mu^-) \leq 6.2 \times 10^{-9} \ (2\sigma) \\ & 2.9 \times 10^{-4} \leq BR(b \to s\gamma) \leq 3.87 \times 10^{-4} \ (2\sigma) \\ & 0.15 \leq \frac{BR(B_u \to \nu_\tau\tau)_{MSSM}}{BR(B_u \to \nu_\tau\tau)_{SM}} \leq 2.41 \ (3\sigma) \end{aligned} \tag{5}$$

Note that the mass bound on the gluino listed above is relaxed in compared to the current bounds ($m_{\tilde{g}} \geq 1.9$ TeV [60]). Analyses for the exclusion limit on the gluino mass are based on the processes in which gluino directly decays into the lightest (or the second lightest) neutralino and chargino. Such processes are expected to be significant especially when the gluino is the next to LSP (NLSP), or the mass difference between the gluino and neutralino (chargino) is not enough to place another supersymmetric particle in the decay cascades. In our work, since we focus on the solutions with $m_{\tilde{t}_1} \lesssim 700$ GeV, the $\tilde{g} \to q\tilde{q}$ can take place in the gluino decay patterns [61]; and consequently the exclusion limit can be slightly reduced since $\text{BR}(\tilde{g} \to q\bar{q}\tilde{\chi}_i^0) \neq 1$. Even though one should not expect a significant reduction by including the stop in the decay cascades, another reduction may be applied due to the theoretical errors in calculation of the supersymmetric mass spectrum, which may allow a few percent deviation from the exclusion limit while selecting the benchmark points. Another reason to reduce the bound on the gluino mass to 1 TeV arises from the gluino contribution to the stop mass through the renormalization group equations (RGEs) [20]. In our work we want to analyze the impact of the LHC exclusion limits on the stop when it is as light as possible, even if such solutions are already excluded by the gluino mass bound. The aim is to scrutinize the exclusion capability of the detector analyses over the stop at each mass scale in the range from about 200–700 GeV. Although these analyses are quite comprehensive when the models are considered only at the low scale without being concerned about the high scale origin, the exclusion picture might be different when the models are constrained from the GUT scale, where all the physical observables can be related to each other and calculated in terms of a few free parameters. In doing this, we apply the gluino mass bound as listed in Eq. (5), but we will try to find the solutions with the gluino as heavy as possible, when we proceed in our analyses by considering benchmark points.

One of the strongest constraints comes from rare B-meson decay into a muon pair. The supersymmetric contributions to the $BR(B_s \to \mu^+\mu^-)$ are severely constrained, since

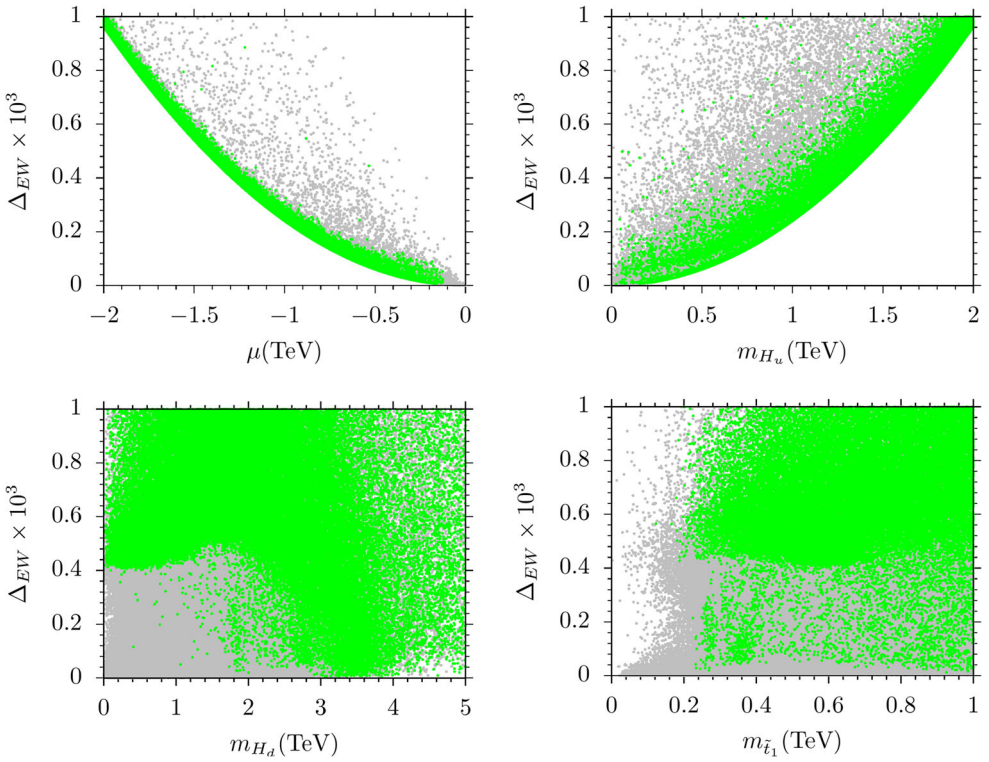

Fig. 1 Plots in $\Delta_{EW} - \mu$, $\Delta_{EW} - m_{H_u}$, $\Delta_{EW} - m_{H_d}$, and $\Delta_{EW} - m_{\tilde{t}}$ planes. All points are consistent with REWSB and neutralino LSP. Gray points are excluded by the current experimental bounds, while the green points are allowed.

the SM's predictions almost overlap with its experimental measurements. Supersymmetric contributions to this process are proportional to $(\tan\beta)^6/m_A^4$. Therefore, it has a strong impact on the regions with large $\tan\beta$ that CP-odd Higgs boson has to be heavy enough ($m_A \sim$ TeV) to suppress the supersymmetric contribution. In addition, the measurements for the $b \to s\gamma$ and $B_u \to \tau\nu$ decay processes have been employed as constraints in our analyses. In computing the branching ratios of the relevant decays, SPheno is interfaced with Flavor Kit [62] provided by SARAH [34].

Finally, we also require the solutions to do no worse than the SM in regard of the muon $g-2$ by requiring $\Delta a_\mu \geq 0$.

4 Fine-tuning and sparticle mass spectrum in MSSM

In this section, we present our results for the fine-tuning and the stop mass and highlight if there is any correlation between them. The acceptable fine-tuning amount can be applied conventionally as $\Delta_{EW} \leq 10^3$. Figure 1 represents our results with plots in $\Delta_{EW} - \mu$, $\Delta_{EW} - m_{H_u}$, $\Delta_{EW} - m_{H_d}$, and $\Delta_{EW} - m_{\tilde{t}}$ planes. All points are consistent with REWSB and neutralino LSP. Gray points are excluded by the current experimental bounds, while the green points are allowed.The $\Delta_{EW} - \mu$ plane reveals a strong correlation between the fine-tuning and the μ-term, which is seen as a tight parabolic curve. According to these results, the required amount of fine-tuning is beyond the acceptable range when $|\mu| \gtrsim 2$ TeV. A similar correlation can be also realized between Δ_{EW} and m_{H_u}, despite not being as strict as that for the $\mu-$term. The result in the $\Delta_{EW} - m_{H_u}$ plane is the impact of the correct EW symmetry breaking scale condition which requires $\mu \approx m_{H_u}$. The $\Delta_{EW} - m_{H_d}$ plane does not show any correlation between Δ_{EW} and m_{H_d}, as discussed before that m_{H_d} is not very strong in calculating the fine-tuning. Surprisingly, the fine-tuning results do not exhibit a strong correlation with the stop mass as seen from the $\Delta_{EW} - m_{\tilde{t}}$ plane, and it is possible to realize the stop as light as about 200 GeV with very low fine-tuning measures (~ 0).

Figure 2 displays the results with plots in the $\Delta_{EW} - \tan\beta$ and $\Delta_{EW} - m_h$ planes. The color coding is the same as Fig. 1. In addition, the purple points form a subset of green and they represent the solutions with $m_{\tilde{t}_1} \leq 700$ GeV. We do not apply the Higgs mass bound in the $\Delta_{EW} - m_h$ plane, since it is represented in one axis. We use rather vertical lines which show the experimental bounds on the Higgs boson mass. The $\Delta_{EW} - \tan\beta$ plane exhibits a restriction in $\tan\beta$ range that this parameter cannot take a value greater than 50. On the other hand, this restriction on this parameter does not arise from the fine-tuning condition, it is rather related to the REWSB condition. In the allowed range it is possible to obtain low fine-tuning for any value of $\tan\beta$.

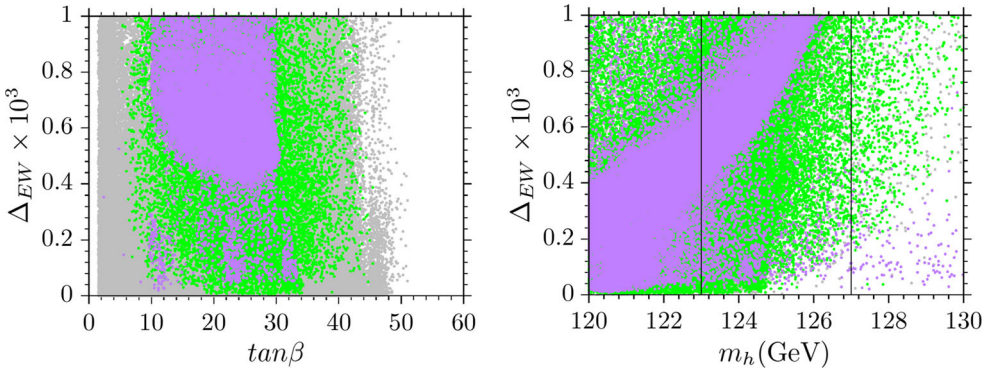

Fig. 2 Plots in $\Delta_{EW} - \tan\beta$ and $\Delta_{EW} - m_h$ planes. The color coding is the same as Fig. 1. In addition, the purple points form a subset of green and they represent the solutions with $m_{\tilde{t}_1} \leq 700$ GeV. We do not apply the Higgs mass bound in the $\Delta_{EW} - m_h$ plane, since it is represented in one axis. We use rather vertical lines which shows the experimental bounds on the Higgs boson mass.

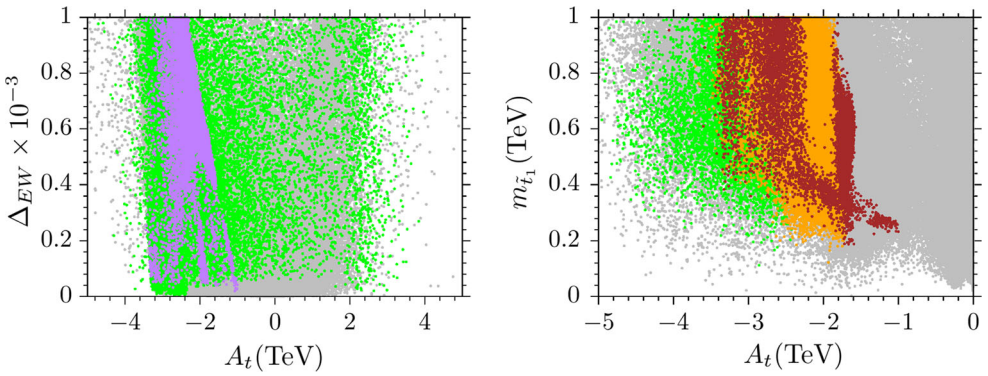

Fig. 3 Plots in $\Delta_{EW} - A_t$ and $m_{\tilde{t}_1} - A_t$ planes. The color coding in the left panel is the same as Fig. 1. While the meaning of gray and green are the same in the right panel, the orange points represents the solutions with $\Delta_{EW} \leq 10^3$, and the brown points form a subset of orange with $\Delta_{EW} \leq 500$. The condition $m_{\tilde{t}_1} \leq 700$ GeV is not applied in the right panel, since the stop mass is represented directly in one axis.

If we consider the solutions with $m_{\tilde{t}_1} \lesssim 700$ GeV (purple), such solutions restrict $\tan\beta$ as $10 \lesssim \tan\beta \lesssim 30$. This bound rather arises due to the negative loop contributions from the bottom sector discussed earlier. Such negative contributions require a heavier stop mass in order to be canceled and yield the Higgs boson of mass about 125 GeV. The $\Delta_{EW} - m_h$ plane shows that the solutions in their statistical distribution exhibit a tendency that the fine-tuning could be zero if the Higgs boson mass was observed to be about 120 GeV. Also, the statistically dense branch shows a linear increase with the Higgs boson mass. However, the fundamental parameter space is spanned by the six free parameters; thus, it is still possible to find some solutions which do not respect the general tendency in the distribution. Despite massive scanning over the parameter space, such solutions are displayed with scattered points in the plots rather than exhibiting a smooth statistical distribution. We have also realized a region of the scattered points in which Δ_{EW} remains between about $40-300$ while the Higgs boson mass increases.

Even though the fine-tuning measurement defined in Eq. (2) does not explicitly depend on A_t and the stop mass, these two parameters are still effective through the loop contributions to m_{H_d} and m_{H_u} denoted as Σ_d and Σ_d in Eq. (1) respectively. Figure 3 displays the impact of the low fine-tuning condition on these parameters in the $\Delta_{EW} - A_t$ and $m_{\tilde{t}_1} - A_t$ planes. The color coding in the left panel is the same as Fig. 1. While the meaning of gray and green are the same in the right panel, the orange points represent solutions with $\Delta_{EW} \leq 10^3$, and brown points form a subset of orange with $\Delta_{EW} \leq 500$. The condition $m_{\tilde{t}_1} \leq 700$ GeV is not applied in the right panel, since the stop mass is represented directly in one axis. As is seen from the $\Delta_{EW} - A_t$ plane, the low fine-tuning condition restricts A_t into a very arrow range from about 1–4 TeV in the negative region. Even though it might be small in the positive region, there is no solution which is compatible with the low fine-tuning and $m_{\tilde{t}_1} \leq 700$ GeV conditions simultaneously. When A_t changes its sign from negative to positive, its effect in the stop mixing is also reversed, and seeking for solutions with low fine-tuning in the

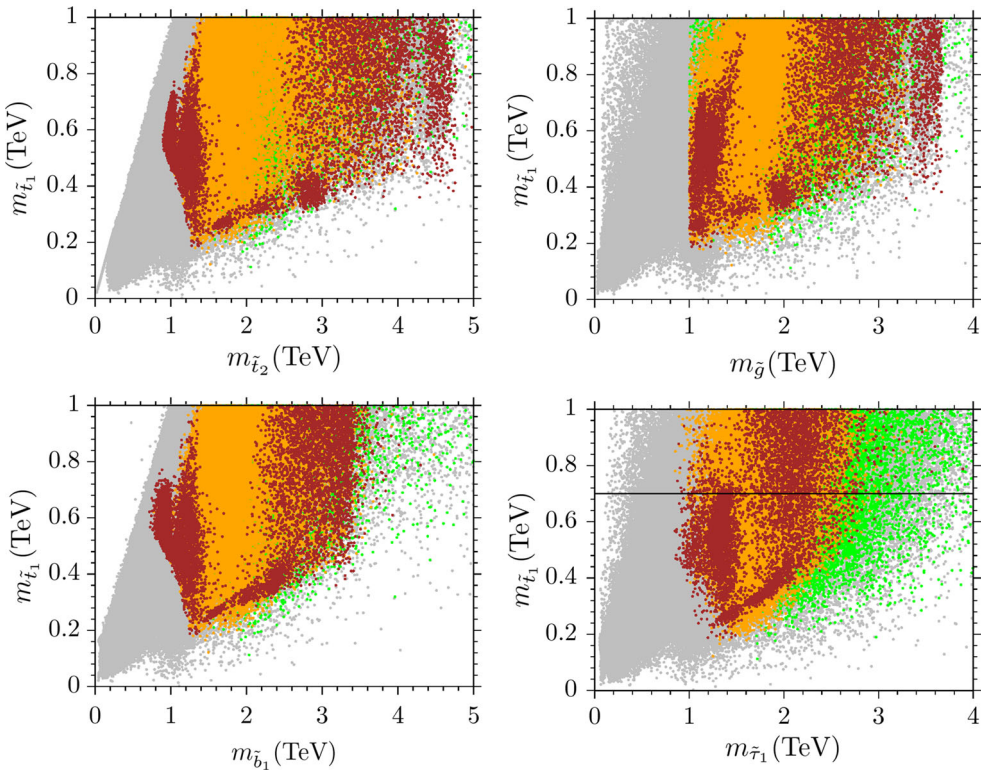

Fig. 4 The sparticle masses in $m_{\tilde{t}_1} - m_{\tilde{t}_2}$, $m_{\tilde{t}_1} - m_{\tilde{g}}$, $m_{\tilde{t}_1} - m_{\tilde{b}_1}$, and $m_{\tilde{t}_1} - m_{\tilde{\tau}_1}$. The color coding is the same as the right panel of Fig. 3.

positive A_t region requires heavier stops ($m_{\tilde{t}_1} \gtrsim 700$ GeV). A previous study has shown that light stop solutions in the positive A_t regions need to be highly fine-tuned ($\Delta_{EW} > 10^3$) [19]. Even though the low scale fine-tuning condition has a strong impact on A_t term, its impact on the stop mass does not seem very strong, and the low fine-tuned solutions (browns with $\Delta_{EW} \leq 500$) can be realized in a wide range of the stop mass as shown up to 1 TeV in the $m_{\tilde{t}_1} - A_t$ plane. In this sense, the correlation between the fine-tuning and A_t is much stronger than that with the stop mass, and with the help of A_t it is possible to realize low fine-tuning for a wide range of the stop mass.

5 Sparticle mass spectrum

In this section, we consider the mass spectrum of the supersymmetric particles in addition to the stop, since they are also of special importance in exploring the low energy implications of MSSM. Figure 4 represents masses of stop, gluino, sbottom and stau with plots in the $m_{\tilde{t}_1} - m_{\tilde{t}_2}$, $m_{\tilde{t}_1} - m_{\tilde{g}}$, $m_{\tilde{t}_1} - m_{\tilde{b}_1}$, and $m_{\tilde{t}_1} - m_{\tilde{\tau}_1}$ planes. The color coding is the same as the right panel of Fig. 3. According to the results represented in the $m_{\tilde{t}_1} - m_{\tilde{t}_2}$ plane, the second stop cannot be lighter than about a TeV, although the lightest stop can be as light as about 200 GeV. When one of the stops is light, the Higgs boson mass constraint pushes the second stop mass up to the TeV scale or above, which also requires a large mixing in the stop sector. In addition to the mixing, gluino can also lead to heavy stop, since it contributes radiatively to the stop mass. The $m_{\tilde{t}_1} - m_{\tilde{g}}$ shows that the stop can be as light as 200 GeV when $m_{\tilde{g}} \sim 1$ TeV. The increase in the stop mass with increasing gluino mass can be seen from the results. However, heavier gluino mass can provide only a slight increase, and it is still possible to realize $m_{\tilde{t}_1} \gtrsim 250$ (brown) GeV, when $m_{\tilde{g}} \gtrsim 1.9$ TeV. Similarly sbottom and stau cannot be lighter than about 1 TeV, when $m_{\tilde{t}_1} \lesssim 400$ GeV as seen from the bottom panels of Fig. 4. However, it is possible to realize the sbottom and stop masses below a TeV as $m_{\tilde{b}_1} \gtrsim 700$ GeV when $m_{\tilde{t}_1} \sim 600$ GeV.

Nearly degenerate stop and sbottom when $m_{\tilde{t}_1} \simeq m_{\tilde{b}_1} \approx$ 600 GeV.

Figure 5 shows the masses of the lightest neutralino and the lightest chargino with plots in the $m_{\tilde{t}_1} - m_{\tilde{\chi}_1^0}$, $m_{\tilde{t}_1} - m_{\tilde{\chi}_1^\pm}$ planes. The color coding is the same as the right panel of Fig. 3. The diagonal line indicates the mass degeneracy between the plotted particles. These two supersymmetric particles play a crucial role, since they take part in stop decay cascades, and the strictest constraints from the direct search at the LHC are based on the decay channels involving the neutralino and chargino. Since we accept only the solutions yielding one of the neutralinos to be LSP, the final states of stop decays should

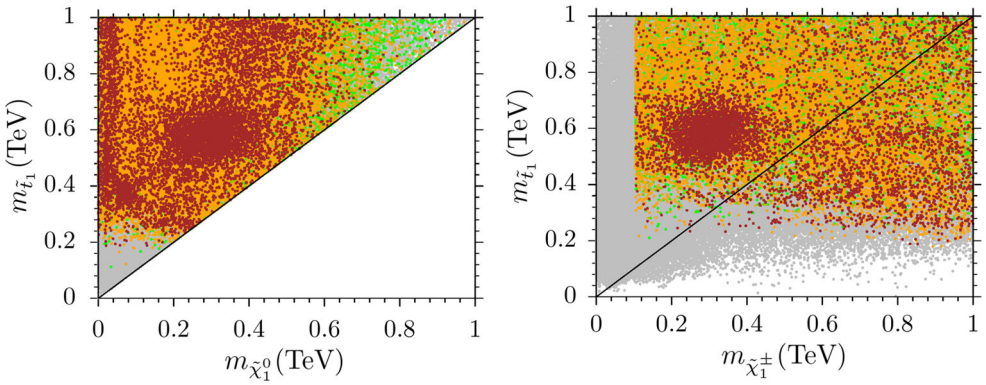

Fig. 5 Plots in the $m_{\tilde{t}_1} - m_{\tilde{\chi}_1^0}, m_{\tilde{t}_1} - m_{\tilde{\chi}_1^\pm}$ planes. The color coding is the same as the right panel of Fig. 3. The diagonal line indicates the mass degeneracy between the plotted particles.

include the neutralino. As mentioned before, the strongest bound on the stop mass is provided from the $\tilde{t} \to t\tilde{\chi}_1^0$ processes, and this decay channel is kinematically allowed only when $m_{\tilde{t}_1} \gtrsim m_{\tilde{\chi}_1^0} + m_t$. The $m_{\tilde{t}_1} - m_{\tilde{\chi}_1^0}$ plane shows that the LSP neutralino can be even almost massless, and hence the $\tilde{t} \to t\tilde{\chi}_1^0$ can be realized even when $m_{\tilde{t}_1} \sim 200$ GeV. A similar discussion can be followed when stop decays into a bottom quark and chargino, which bounds the stop mass as $m_{\tilde{t}} \gtrsim 650$ GeV [7]. Indeed this channel is the best option to analyze and exclude the stop solutions below some scales. The lightest chargino mass is realized as low as about 100 GeV as seen from the $m_{\tilde{t}_1} - m_{\tilde{\chi}_1^\pm}$ plane. Since the mass of the bottom quark is negligible in compared to the stop and chargino masses, the $\tilde{t} \to b\tilde{\chi}_1^0$ can be realized even when the stop and chargino are nearly degenerate in mass.

Before concluding, our study focuses on the regions where the stop is realized lighter than 700 GeV, which are excluded by the current LHC results. In the next section we consider such solutions over some benchmark points and analyze the exclusion impact by comparing the implications with the ATLAS and CMS analyses. Despite the confidentiality of such strict constraints over the low scale analyses, some assumptions behind such experimental analyses may not be fulfilled when the parameter space is constrained from the GUT scale. For instance, even though the best exclusion channel is $\tilde{t} \to b\tilde{\chi}_1^0$, the chargino in this process should eventually decay into the neutralino along with appropriate SM particles, and the strict exclusion arises when chargino decays into a W-boson and LSP neutralino. The stop and chargino decays can be linked to each other easily in the low scale considerations, since a large set of low scale free parameters of MSSM allows such freedom. On the other hand, the SUSY GUTs have only a few free parameters, and these two processes cannot be set freely, but they are calculated in certain correlations. Thus, even when it is possible to find some solutions in which $\mathrm{BR}(\tilde{t} \to b\tilde{\chi}_1^\pm) \sim 1$, the chargino may not be kinematically allowed to decay into a W-boson and LSP neutralino. In such cases, the largest branching ratio can be found for the processes in which the chargino decay into $u\bar{d}\tilde{\chi}_1^0$. Such processes cannot provide strict constraints due to large uncertainties in the QCD sector.

6 LHC escape of light stops

In this section, we discuss the possibility of the light stop solutions to survive or being excluded over some benchmark points. We consider the processes in which stop decays into either a top quark and LSP neutralino, or a bottom quark and chargino, which are the main channels in exclusion analyses. The latter processes have a large impact in excluding the light stop solutions when the chargino is allowed to decay into $W^\pm$ along with the LSP neutralino. As discussed before, SUSY GUTs can yield solutions which react different in such exclusive analyses, since some low scale fundamental parameters, such as mixings, masses, couplings of supersymmetric particles relevant to the analyzed processes, are determined and constrained by a few GUT scale fundamental parameters.

To investigate the impact of the negative results from the direct searches we follow similar analyses represented in [52]. Generating events for the signals and relevant background processes are performed by using MadGraph [63]. We then transfer the generated event files to Delphes [64] to employ the detector response. Finally, the results are plotted by using MadAnalysis [65]. We also apply some cuts to suppress the background, which are also employed in the analyses represented in [52]. These cuts can be listed as follows:

- $E_{\mathrm{T}}^{\mathrm{miss}} > 100$ GeV, $M_T > 120$ GeV,
- $P_T > 30$ GeV and $|\eta| < 2.4$ for jets,
- $P_T > 30(25)$ GeV and $|\eta| < 1.422(2.1)$ for electrons (muons),
- $P_T^{\mathrm{total}} < \min(5\ \mathrm{GeV}, 0.15 P_T^l)$,

- $\Delta R(j,l) > 0.4$.

where $E_T^{\rm miss}$ is the missing transverse energy, while M_T represents the transverse mass, and P_T stands for the transverse momentum. If one considers the cone of radius $R = \sqrt{\eta^2+\phi^2}$ in terms of pseudorapidity (η) and azimuthal angle (ϕ), in which the particles flow, $\Delta_R(l,j)$ can be a useful cut to isolate leptons (l) from the jets (j). ΔR parameter may provide a useful tool to isolate the leptons from the jets. It is defined as $\Delta R = \sqrt{(\Delta\eta)^2+(\Delta\phi)^2}$, where η stands for the pseudorapidity and ϕ is the azimuthal angle. The cut on this parameter as $\Delta R(j,l) > 0.4$ is applied to remove the events in which the leptons and jets overlap.

Both signal processes end up with the final cases involving a pair of each b quark, charged lepton, neutrino and LSP neutralino. The signal processes have to include LSP neutralinos, since R-parity is conserved. The relevant background has a final state of all these particles except neutralino. Only a pair of neutrinos contributes to the missing energy in the background process, also the neutralinos contribute in the signals; and hence the cut on $E_T^{\rm miss}$ is useful to suppress the background. In addition, since there are more particles in the final states of signals, the transverse mass is expected to be greater than that of the background process. The cuts on the transverse momentum P_T makes possible to isolate the leptons and $\Delta R(j,l) > 0.4$ prevent them to overlap with the jets. Even though we do not apply a specific cut on P_T of b quarks ($P_T^{(b)}$), $P_T^{(b)}$ is expected to be greater for the signals than the background.

The challenge in detecting the stop is that it yields quite similar final state configuration to those involving a top quark. Thus, despite the discussion about the cuts above, suppressing the background results in also significant suppression in the signal as well. We will consider two signal processes separately next, and discuss the overall results for the stop detection in details. Our analyses are performed for the collisions with 13–14 TeV center of mass (COM) energy, and we set the luminosity to 19.5 fb^{-1}. Note that setting the COM energy 13 or 14 TeV does not yield any visible difference in the results; hence, we present our results for both 13–14 TeV COM energy.

6.1 $\tilde{\mathbf{t}} \to \mathbf{t}\tilde{\chi}_1^0$

We first discuss the process $pp \to \tilde{t}\bar{\tilde{t}}^* \to t\bar{t}\tilde{\chi}_1^0\tilde{\chi}_1^0 \to b\bar{b}W^\pm W^\mp\tilde{\chi}_1^0\tilde{\chi}_1^0 \to b\bar{b}l^\pm\bar{l}^\mp\nu_l\nu_l\tilde{\chi}_1^0\tilde{\chi}_1^0$ over some benchmark points within $200 \lesssim m_{\tilde{t}} \lesssim 700$ GeV given in Table 1. All points are consistent with the current experimental results. All masses are in GeV unit, while the cross-sections are given in pb. As seen, all points predict BR$(\tilde{t} \to)t\tilde{\chi}_1^0 \sim 1$ and hence $m_{\tilde{t}-m_{\tilde{\chi}_1^0}} \geq m_t$. The relevant background process is $pp \to t\bar{t} \to b\bar{b}W^\pm W^\mp \to b\bar{b}l^\pm\bar{l}^\mp\nu_l\nu_l$.

Figure 6 represents the $E_T^{\rm miss}$ and M_T for the signals and background. The cut on $E_T^{\rm miss}$ (M_T) is not applied on the left (right) panel. As seen from the left panel, the cross-section for the most striking signal with $m_{\tilde{t}} \sim 290$ GeV is still about three orders of magnitude smaller than the background, which leads to a small significance for the signal. As expected, the cross-section diminishes with the stop mass increasing. Even though the missing energy might be expected to be low for the background process, the energetic neutrinos can cause large missing energy, and it can be much larger than the cut applied on $E_T^{\rm miss}$. If one strengthens the cut on the missing energy as $E_T^{\rm miss} \lesssim 325$ GeV, then the background can be removed significantly. However, the number of events in this region is $\lesssim 1$, and it is not enough for detection or exclusion at a high CL. Similar discussion can also be followed for the transverse mass as displayed in the right panel of Fig. 6. While a cut on M_T applied as $M_T > 400$ GeV can remove the background, the signal processes cannot provide observable tracks, either. In this context, the cuts applied to suppress the background also suppress the signals significantly, and they result in quite a few number of events, which makes signals difficult to detect.

The benchmark points considered as possible signals within $200 \lesssim m_{\tilde{t}} \lesssim 700$ GeV are listed in Table 1. All points are chosen as being consistent with the current experimental results. All masses are in GeV unit, while the cross-sections are given in pb. As is seen, the solutions can predict BR$(\tilde{t}_1 \to t\tilde{\chi}_1) \sim 1$, for a stop mass as low as 287 GeV, while the gluino mass is found to be allowed by the current exclusion limit. All points allow stop only to decay a top quark and LSP neutralino with the cross-section in a range as $10^{-3} \lesssim \sigma(\text{signal}) \lesssim 10^{-1}$ pb. Although the benchmark points fulfill the assumption that is BR$(\tilde{t} \to t\tilde{\chi}_1^0) \sim 1$, they can be excluded only up to about 60% CL for $m_{\tilde{t}} \lesssim 500$ GeV, while the exclusion cannot exceed a few percentage for $m_{\tilde{t}} \gtrsim 500$ GeV.

6.2 $\tilde{\mathbf{t}} \to \mathbf{b}\tilde{\chi}_1^\pm$

We follow a similar analyses for the decay channel in which stop decays into a b quark and a chargino. The signal process can be expressed as $pp \to \tilde{t}\bar{\tilde{t}}^* \to b\bar{b}\tilde{\chi}_1^\pm\tilde{\chi}_1^\pm \to b\bar{b}W^\pm W^\pm\tilde{\chi}_1^0\tilde{\chi}_1^0 \to b\bar{b}l^\pm\bar{l}^\pm\nu_l\bar{\nu}_l\tilde{\chi}_1^0\tilde{\chi}_1^0$. In this case, it is not enough to have stop largely decay into a b quark and the chargino, since the chargino should also be allowed to decay into a W-boson and neutralino. If it is not allowed, the exclusion on the stop is not too much strict. The relevant background is the same as given for the previous signal processes.

Figure 7 displays the plots for the $E_T^{\rm miss}$ and M_T for the signals and background. The cut on $E_T^{\rm miss}$ (M_T) is not applied on the left (right) panel. A similar conclusion can be derived also for this type of signal processes, since suppressing the background does not leave enough number of events for the

Table 1 Benchmark points for $\tilde{t} \to t\tilde{\chi}_1^0$ with several mass scales of the stop from about 287 to 683 GeV

	Point 1	Point 2	Point 3	Point 4	Point 5
m_0	1773	2193	2551	2956	3164
M_1	− 149.3	− 126.9	− 295.5	− 827.6	− 1006
M_2	− 2848	− 3642	− 3904	− 6088	− 6290
M_3	795.8	800.8	882.3	1477	1519
$\tan\beta$	19.64	25.25	29.81	31.38	31.35
A_0/m_0	− 2.881	− 2.384	− 2.432	− 2.746	− 2.708
μ	− 1371	− 737.3	− 1123	799.1	− 1043
$\Delta_{\rm EW}$	485.6	169.0	339.8	209.2	314.5
m_h	123.05	122.81	123.11	124.39	124.89
m_H	2571	2750	2812	3625	3782
m_A	2571	2750	2812	3625	3782
$m_{H^\pm}$	2572	2751	2812	3626	3783
$m_{\tilde{\chi}^0_{1,2}}$	**66.76, 1380**	**55.82, 743.2**	**131.52, 1135**	**376.2, 808.9**	**459.2, 1055**
$m_{\tilde{\chi}^0_{3,4}}$	1383, 2369	744.3, 3023	1136, 3247	810.1, 5063	1056, 5186
$m_{\tilde{\chi}^\pm_{1,2}}$	**1380, 2369**	**742.3, 3024**	**1134, 3247**	**807.9, 5063**	**1054, 5185**
$m_{\tilde{g}}$	1919	1962	2150	3403	3498
$m_{\tilde{u}_{L,R}}$	2938, 2322	3498, 2641	3875, 3006	5468, 3951	5664, 4145
$m_{\tilde{t}_{1,2}}$	**287.15, 2313**	**396.17, 2637**	**490.29, 3013**	**583.81, 3960**	**683.82, 4162**
$m_{\tilde{d}_{L,R}}$	2938, 2323	3498, 2642	3875, 3006	5468, 3949	5664, 4142
$m_{\tilde{b}_{1,2}}$	2129, 2313	2334, 2637	2477, 3012	3216, 3957	3369, 4157
$m_{\tilde{\nu}_{e,\mu}}$	2536, 2536	3186, 3186	3548, 3547	4828, 4827	5022, 5021
$m_{\tilde{\nu}_\tau}$	2461	3069	3357	4579	4759
$m_{\tilde{e}_{L,R}}$	2536, 1770	3186, 2189	3548, 2548	4828, 2965	5022, 3178
$m_{\tilde{\tau}_{1,2}}$	1570, 1770	1863, 2189	1996, 2548	2101, 2965	2285, 3178
$BR(\tilde{t}_1 \to \tilde{\chi}^0_1 t)$	1	1	1	1	1
$BR(\tilde{t}_1 \to \tilde{\chi}^\pm_1 b)$	0	0	0	0	0
$BR(\tilde{\chi}^\pm_1 \to \tilde{\chi}^0_1 W^\pm)$	3.4×10^{-2}	5.86×10^{-2}	4.6×10^{-2}	1.2×10^{-1}	8.7×10^{-2}
σ(signal)	$\mathbf{2.46 \times 10^{-1}}$	$\mathbf{4.544 \times 10^{-2}}$	$\mathbf{1.375 \times 10^{-2}}$	$\mathbf{4.883 \times 10^{-3}}$	$\mathbf{1.855 \times 10^{-3}}$
$\sigma(pp \to \tilde{t}\tilde{t}^*)$	**7.115**	**1.314**	$\mathbf{4.018 \times 10^{-1}}$	$\mathbf{1.545 \times 10^{-1}}$	$\mathbf{5.523 \times 10^{-2}}$
Exclusion CL%	49.7	59.5	46.6	5.5	3.6

All points are chosen as being consistent with the current experimental results. All masses are in GeV unit, while the cross-sections are given in pb

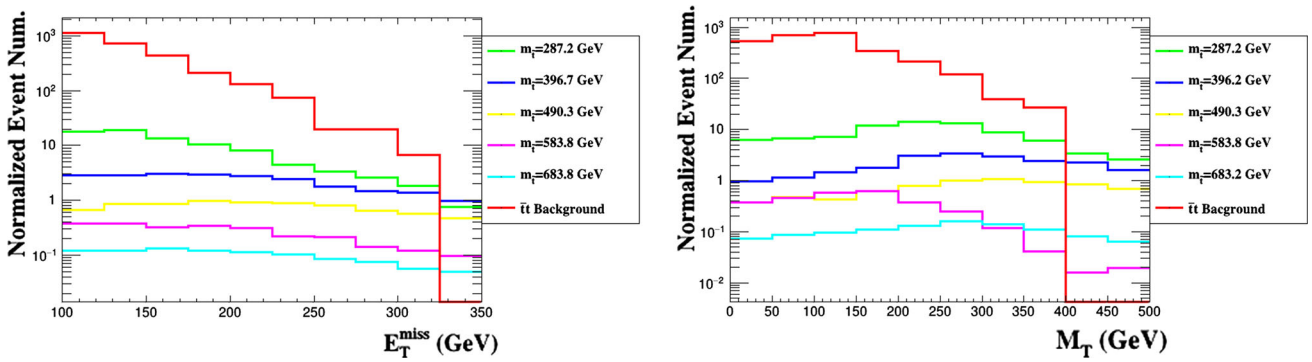

Fig. 6 Plots representing the $E_T^{\rm miss}$ and M_T for the signals and background. The cut on $E_T^{\rm miss}$ (M_T) is not applied on the left (right) panel.

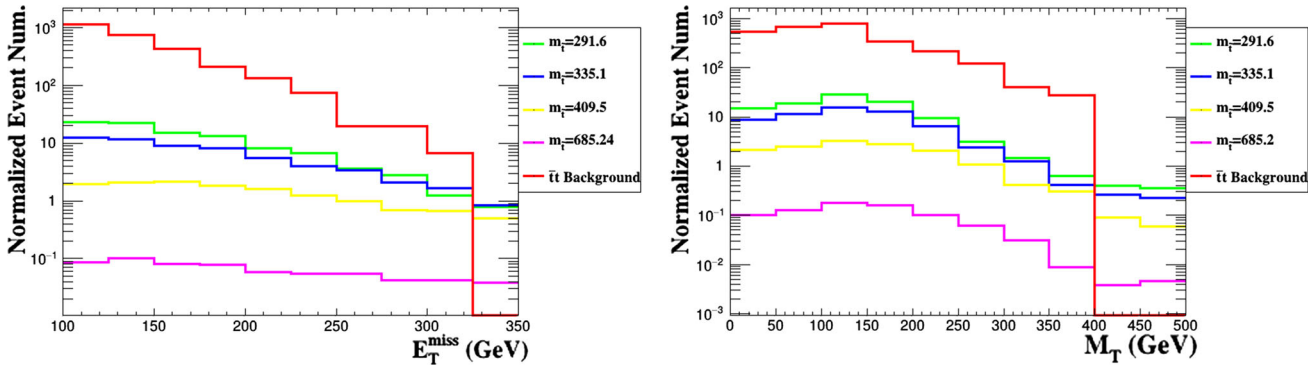

Fig. 7 Plots representing the E_T^{miss} and M_T for the signals and background. The cut on E_T^{miss} (M_T) is not applied on the left (right) panel.

signal. In this context, the background mostly suppresses the signal processes and it is not possible to remove the background while keeping the signal processes intact.

The details for the benchmark points considered as a possible signal are given in Table 2 within $200 \lesssim m_{\tilde{t}} \lesssim 700$ GeV. All points are chosen as being consistent with the current experimental results. All masses are in GeV unit, while the cross-sections are given in pb. All points are chosen to yield the largest branching ratio for $\tilde{t} \to b\tilde{\chi}_1^{\pm}$. Note that we do not find any solution for $500 < m_{\tilde{t}} < 600$ GeV which allows large $\text{BR}(\tilde{\chi}_1^0 \to W^{\pm}\tilde{\chi}_1^0)$. In addition, even though we tried to respect to the gluino mass bound in selecting the benchmark points in Table 2, it was not possible to find stop mass in the desired ranges (the first and third points in Table 2). For the mass scales indicated with these benchmark points, such points can be reanalyzed with respect to the gluino production and decay processes including stop, since they predict the gluino mass slightly below the exclusion limit. Considering the theoretical errors in calculating the gluino mass and the assumption of non-observed stop, such points may still be testable, and they require more thorough analyses before being excluded. The cross-section for the signal changes from $\sim 10^{-1}$ to $\sim 10^{-3}$ pb. The exclusion can be as significant as about 45% CL for $m_{\tilde{t}} \lesssim 500$ GeV, while excluding is not possible (by neglecting 1% CL) for $m_{\tilde{t}} \gtrsim 500$ GeV.

We consider the the decay channels which provide the strongest constraints on the stop mass, and we realized that the exclusion can be as good as only at 50–60% CL. If one considers the 65% CL as to be potentially observable signal and 95% CL to be pure exclusion limit, the solutions with lighter stop mass can still have a chance to survive under the current collider analyses. Note that we set the luminosity close to its current values reached by the experiments. The number of events for the signals and consequently their exclusion level will raise with the increasing luminosity, and the exclusion will be more severe near future.

Before concluding this section, one also needs to discuss the reason why the cross-sections for the signals are at least three orders of magnitude smaller than the background, despite the large branching ratios for the relevant decays of stops in the chosen benchmark points. The both signal processes start with the stop pair production, while the background include a pair of top quarks whose production cross-section is [66].

$$\sigma(pp \to t\bar{t}) = 818 \pm 8(\text{stat}) \pm 27(\text{syst}) \pm 19(\text{lumi}) \pm 12(\text{beam})\text{pb} \quad (6)$$

Compared to the cross-section given in Eq. (6), the largest cross-section for the stop pair productions are realized as ~ 7 pb for the first points of Tables 1 and 2, which is much smaller even than errors in the production cross-section of the top quark pair. In this context, the stop pair production with a negligible cross-section is the main reason, which reduce the total cross-section in the considered signal processes.

7 Conclusion

We discussed the fine-tuning issue within the MSSM framework. We interpreted the fine-tuning as an indication for missing mechanisms, which can be left out in the minimal supersymmetric models. Following this idea we imposed non-universal gaugino masses at the GUT scale. We showed that the μ-term is the main parameter which determines the required fine-tuning amount, and it is possible to realize $\Delta_{EW} \approx 0$ consistently with the EW breaking. Even though μ is the main parameter, it also has an impact on the SSB Higgs field mass, m_{H_u}, since $\mu \approx m_{H_u}$ is required to have the EW breaking at the correct scale ($M_Z \sim 90$ GeV). On the other hand, m_{H_d} has almost no impact on the fine-tuning measurements, since its contributions are suppressed by $\tan\beta$. Any value of $\tan\beta$ can yield an acceptable amount of fine-tuning, but it is restricted to the range 10-30, if one also requires the solutions to yield light stop masses ($m_{\tilde{t}} \leq 700$ GeV). Even

Table 2 Benchmark points for $\tilde{t} \to b\tilde{\chi}_1^{\pm}$ with several mass scales of the stop from about 291 to 685 GeV

	Point 1	Point 2	Point 3	Point 4
m_0	1755	2062	2286	2925
M_1	− 151.8	− 182.8	− 135.2	− 1206
M_2	− 3142	− 3799	− 3732	− 6053
M_3	667.4	827.7	754.9	1467
$\tan\beta$	22.6	22.4	23.7	31.54
A_0/m_0	− 2.33	− 2.38	− 2.20	− 2.723
μ	− 189.0	− 216.9	− 236.7	− 641.8
$\Delta_{\rm EW}$	40.7	56.7	52.8	139.4
m_h	123.0	124.2	124.2	124.21
m_H	2350	2808	2872	3580
m_A	2350	2808	2872	3580
$m_{H^{\pm}}$	2351	2808	2872	3580
$m_{\tilde{\chi}^0_{1,2}}$	**61.0, 179.5**	**75.7, 202.9**	**56.2, 226.2**	**541.1, 651.1**
$m_{\tilde{\chi}^0_{3,4}}$	184.6, 2599	208.2, 3150	228.7, 3098	660.4, 5032
$m_{\tilde{\chi}^{\pm}_{1,2}}$	**173.7, 259.9**	**198.0, 3150**	**221.2, 3098**	**649.7, 5032**
$m_{\tilde{g}}$	1656	2014	1871	3382
$m_{\tilde{u}_{L,R}}$	2938, 2159	1113, 2573	1124, 2268	5417, 3912
$m_{\tilde{t}_{1,2}}$	**291.6, 2149**	**335.1, 2558**	**409.5, 2666**	**685.24, 3934**
$m_{\tilde{d}_{L,R}}$	2938, 2160	1113, 2575	1124, 2669	5417, 3906
$m_{\tilde{b}_{1,2}}$	1965, 2149	2344, 2558	2419, 2665	3194, 3927
$m_{\tilde{\nu}_{e,\mu}}$	2667, 2666	1005, 1005	1041, 1041	4790, 4789
$m_{\tilde{\nu}_{\tau}}$	2589	3086	3191	4550
$m_{\tilde{e}_{L,R}}$	2667, 1751	1005, 2058	1041, 2282	4790, 2951
$m_{\tilde{\tau}_{1,2}}$	1548, 1752	1818, 2058	2014, 2282	2105, 2951
$BR(\tilde{t}_1 \to \tilde{\chi}^0_1 t)$	0.08	0.11	0.13	0
$BR(\tilde{t}_1 \to \tilde{\chi}^{\pm}_1 b)$	0.92	0.89	0.7	1
$BR(\tilde{\chi}^{\pm}_1 \to \tilde{\chi}^0_1 W^{\pm})$	1	1	1	1
$\sigma(pp \to \tilde{t}\tilde{t}^*)$	**6.58**	**3.2**	**1.1**	$\mathbf{5.447 \times 10^{-2}}$
σ(signal)	$\mathbf{2.4 \times 10^{-1}}$	$\mathbf{1.1 \times 10^{-1}}$	$\mathbf{2.0 \times 10^{-2}}$	$\mathbf{2.464 \times 10^{-3}}$
Exclusion	42.1% CLs	42.8% CLs	43.3% CLs	1.0% CLs

All points are chosen as being consistent with the current experimental results. All masses are in GeV unit, while the cross-sections are given in pb

though we do not apply a direct bound on the stop mass, the other LHC constraints can bound the stop mass from below. The current results from the rare B-meson decays and the Higgs boson mass do not allow solutions with $m_{\tilde{t}} \lesssim 200$ GeV. In addition, the gluino mass bound ($m_{\tilde{g}} \geq 1.9$ TeV) excludes those with $m_{\tilde{t}} \lesssim 250$ GeV, when the fine-tuning condition is applied as $\Delta_{EW} \leq 500$. However, it is still possible to realize $m_{\tilde{t}} \lesssim 400$ GeV, when $m_{\tilde{g}} \sim 3.7(8)$ TeV. We also observe that the mixing in the stop sector parametrized with A_t has stronger impact than the stop mass itself on the required fine-tuning such that Δ_{EW} remains almost the same with constant A_t, even if the stop mass increases. In addition to the stop and gluino, sbottom mass lies from 700 GeV to about 3 TeV. Besides, the low scale mass spectrum yield $m_{\tilde{\tau}} \gtrsim 1$ TeV.

Finally we discussed the detection and exclusion possibility of the stops lighter than 700 GeV over the strict channels in the collider analyses. We chose benchmark points which predict the largest impact on the relevant decay channels within our data. We found that the largest cross-section obtained for a possible signal process is about three magnitude smaller than the background processes. The cuts applied to suppress the background left quite few number of events for the signals, which make the detection or exclusion obscure. The possible exclusion level is at about 60% CL at most for the processes involving $\tilde{t} \to t\tilde{\chi}^0_1$, while it is about 50% for those with $\tilde{t} \to b\tilde{\chi}^{\pm}_1$. These results are valid when $m_{\tilde{t}} \lesssim 500$ GeV, while the exclusion level significantly decreases when $m_{\tilde{t}} \gtrsim 500$ GeV. If one can require the exclusion at 65% CL at least to have a clear signal, these exclusion levels are

still lower, and the solutions with light stops may still have a chance to survive under the current limits. Note that the exclusion could be much more severe, if the model was not constrained from the GUT scale. Despite large branching ratios predicted by the benchmark points, the small cross-section for the signal processes arises from the stop pair production for which $\sigma(pp \to \tilde{t}\tilde{t}^*) \lesssim 7$ pb. Its cross-section is smaller even than the error bars in calculation of $\sigma(pp \to t\bar{t})$. Our analyses represented in this work were performed with 19.5 fb^{-1} luminosity. The number of events for the signal processes will raise with the increasing luminosity; thus, one can conclude the the exclusion will be more severe when the new results are released from near future experiments.

Acknowledgements We would like to thank Qaisar Shafi, Durmuş Ali Demir, Zafer Altın, and Büşra Niş for fruitful discussions. We are also grateful to Jack Araz for useful discussions about LHC analyses. Part of the numerical calculations reported in this paper were performed at the National Academic Network and Information Center (ULAKBIM) of The Scientific and Technological Research Council of Turkey (TUBITAK), High Performance and Grid Computing Center (Truba Resources).

Funded by SCOAP[3].

References

1. G. Aad et al., ATLAS Collaboration. Phys. Lett. B **716**, 1–29 (2012)
2. S. Chatrchyan et al., CMS Collaboration. JHEP **1306**, 081 (2013)
3. M. Carena, S. Gori, I. Low, N.R. Shah, C.E. Wagner, M JHEP **1302**, 114 (2013)
4. S. Heinemeyer, O. Stal, G. Weiglein, Phys. Lett. B **710**, 201 (2012). arXiv:1112.3026 [hep-ph]
5. A. Arbey, M. Battaglia, A. Djouadi, F. Mahmoudi, J. Quevillon, Phys. Lett. B **708**, 162 (2012). arXiv:1112.3028 [hep-ph]
6. The ATLAS Collaboration, ATLAS-CONF-2013-068
7. Outschoorn, V. I. M. [CMS Collaboration] *EPJ Web Conf.* **2013**, *60*, 18003
8. G. Aad *et al.* ATLAS Collaboration, Eur. Phys. J. C **75**, no. 10, 510 (2015) Erratum: [Eur. Phys. J. C **76**, no. 3, 153 (2016)] arXiv:1506.08616 [hep-ex]
9. M. Papucci, J. T. Ruderman, A. Weiler, JHEP **1209**, 035 (2012) arXiv:1110.6926 [hep-ph]
10. J. A. Casas, J. M. Moreno, S. Robles, K. Rolbiecki, B. Zaldvar, JHEP **1506**, 070 (2015) arXiv:1407.6966 [hep-ph]
11. C. Brust, A. Katz, S. Lawrence, R. Sundrum, JHEP **1203**, 103 (2012). arXiv:1110.6670 [hep-ph]
12. H. Baer, V. Barger, N. Nagata, M. Savoy, Phys. Rev. D **95**, no. 5, 055012 (2017) arXiv:1611.08511 [hep-ph]
13. M. Carena, S. Gori, I. Low, N.R. Shah, C.E. Wagner, M JHEP **1203**, 014 (2012)
14. B. Ananthanarayan, P.N. Pandita, Int. J. Mod. Phys. A **22**, 3229–3259 (2007)
15. S. Bhattacharya, A. Datta, B. Mukhopadhyaya, JHEP **0710**, 080 (2007)
16. S.P. Martin, Phys. Rev. D **79**, 095019 (2009)
17. U. Chattopadhyay, D. Das, D.P. Roy, Phys. Rev. D **79**, 095013 (2009)
18. A. Corsetti, P. Nath, Phys. Rev. D **64**, 125010 (2001). and references therein
19. D.A. Demir, C.S. Un, Phys. Rev. D **90**, 095015 (2014)
20. S. P. Martin, Adv. Ser. Direct. High Energy Phys. **21**, 1 (2010) [Adv. Ser. Direct. High Energy Phys. **18**, 1 (1998)] [hep-ph/9709356]
21. U. Ellwanger, C. Hugonie, Phys. Lett. B **457**, 299 (1999). [hep-ph/9902401]
22. I. Gogoladze, B. He, Q. Shafi, Phys. Lett. B **718**, 1008 (2013). arXiv:1209.5984 [hep-ph]
23. I. Gogoladze, B. He, A. Mustafayev, S. Raza, Q. Shafi, JHEP **1405**, 078 (2014). arXiv:1401.8251 [hep-ph]
24. A. Elsayed, S. Khalil, S. Moretti, Phys. Lett. B **715**, 208 (2012). arXiv:1106.2130 [hep-ph]
25. S. Khalil, C.S. Un, Phys. Lett. B **763**, 164 (2016). arXiv:1509.05391 [hep-ph]
26. T. Li, S. Raza and X. C. Wang, Phys. Rev. D **93**, no. 11, 115014 (2016) arXiv:1510.06851 [hep-ph]
27. Y. Hicyilmaz, M. Ceylan, A. Altas, L. Solmaz, C. S. Un, Phys. Rev. D **94**, no. 9, 095001 (2016) arXiv:1604.06430 [hep-ph]
28. I. Gogoladze, F. Nasir, Q. Shafi, Int. J. Mod. Phys. A **28**, 1350046 (2013). arXiv:1212.2593 [hep-ph]
29. I. Gogoladze, F. Nasir, Q. Shafi, JHEP **1311**, 173 (2013). arXiv:1306.5699 [hep-ph]
30. L. Calibbi, T. Li, A. Mustafayev, S. Raza, Phys. Rev. D **93**, no. 11, 115018 (2016) arXiv:1603.06720 [hep-ph]
31. I. Gogoladze, A. Mustafayev, Q. Shafi, C. S. Un, Phys. Rev. D **94**, no. 7, 075012 (2016) arXiv:1609.02124 [hep-ph]
32. W. Porod, Comput. Phys. Commun. **153**, 275 (2003)
33. W. Porod, F. Staub, Comput. Phys. Commun. **183**, 2458 (2012)
34. Staub, F. **2008**, Preprint arXiv:0806.0538
35. F. Staub, Comput. Phys. Commun. **182**, 808 (2011)
36. J. Hisano, H. Murayama, T. Yanagida, Nucl. Phys. B **402**, 46 (1993)
37. J.L. Chkareuli, I.G. Gogoladze, Phys. Rev. D **58**, 055011 (1998)
38. T. E. W. Group, CDF and D0 collaborations, **2009**, Preprint arXiv:0903.2503
39. I. Gogoladze, R. Khalid, S. Raza, Q. Shafi, JHEP **1106**, 117 (2011)
40. I. Gogoladze, Q. Shafi, C.S. Un, JHEP **1208**, 028 (2012)
41. M. Adeel Ajaib, I. Gogoladze, Q. Shafi, C. Un, S. JHEP **1307**, 139 (2013)
42. L.E. Ibanez, G.G. Ross, Phys. Lett. **110B**, 215 (1982)
43. K. Inoue, A. Kakuto, H. Komatsu, S. Takeshita, Prog. Theor. Phys. **68**, 927 (1982)
44. L.E. Ibanez, Phys. Lett. **118B**, 73 (1982)
45. J.R. Ellis, D.V. Nanopoulos, K. Tamvakis, Phys. Lett. **121B**, 123 (1983)
46. L. Alvarez-Gaume, J. Polchinski, M.B. Wise, Nucl. Phys. B **221**, 495 (1983)
47. K. Nakamura et al., Particle data group collaboration. J. Phys. G **37**, 075021 (2010)
48. G. Hinshaw et al., WMAP Collaboration. Astrophys. J. Suppl. **208**, 19 (2013). arXiv:1212.5226 [astro-ph.CO]
49. P.A.R. Ade et al., Planck Collaboration. Astron. Astrophys. **594**, A13 (2016). arXiv:1502.01589 [astro-ph.CO]
50. H. Baer, I. Gogoladze, A. Mustafayev, S. Raza, Q. Shafi, JHEP **1203**, 047 (2012) arXiv:1201.4412 [hep-ph]
51. T. Li, D.V. Nanopoulos, S. Raza, X.C. Wang, JHEP **1408**, 128 (2014). arXiv:1406.5574 [hep-ph]
52. S. Chatrchyan *et al.* [CMS Collaboration], Eur. Phys. J. C **73**, no. 12, 2677 (2013) arXiv:1308.1586 [hep-ex]
53. G. Belanger, F. Boudjema, A. Pukhov, R.K. Singh, JHEP **0911**, 026 (2009)

54. H. Baer, S. Kraml, S. Sekmen, H. Summy, JHEP **0803**, 056 (2008)
55. K.A. Olive et al., Particle Data Group Collaboration. Chin. Phys. C **38**, 090001 (2014)
56. G. Aad *et al.* [ATLAS and CMS Collaborations], Phys. Rev. Lett. **114**, 191803 (2015) https://doi.org/10.1103/PhysRevLett.114.191803. arXiv:1503.07589 [hep-ex]
57. R. Aaij et al., LHCb Collaboration. Phys. Rev. Lett. **110**(2), 021801 (2013)
58. Amhis, Y. *et al.* [Heavy Flavor Averaging Group Collaboration], **2012**, Preprint arXiv:1207.1158
59. Asner, D. *et al.* [Heavy Flavor Averaging Group Collaboration], **2010** , Preprint arXiv:1010.1589
60. A. M. Sirunyan et al. [CMS Collaboration], arXiv:1704.07781 [hep-ex]; The ATLAS collaboration [ATLAS Collaboration], ATLAS-CONF-2017-021
61. N. Nagata, H. Otono, S. Shirai, JHEP **1703**, 025 (2017). arXiv:1701.07664 [hep-ph], and references therein
62. W. Porod, F. Staub, A. Vicente, Eur. Phys. J. C **74**, no. 8, 2992 (2014) https://doi.org/10.1140/epjc/s10052-014-2992-2, arXiv:1405.1434 [hep-ph], and references therein
63. J. Alwall, M. Herquet, F. Maltoni, O. Mattelaer, T. Stelzer, JHEP **1106**, 128 (2011). arXiv:1106.0522 [hep-ph]
64. J. de Favereau et al., DELPHES 3 Collaboration. JHEP **1402**, 057 (2014). arXiv:1307.6346 [hep-ex]
65. E. Conte, B. Fuks, G. Serret, Comput. Phys. Commun. **184**, 222 (2013). arXiv:1206.1599 [hep-ph]
66. M. Aaboud *et al.* [ATLAS Collaboration], Phys. Lett. B **761**, 136 (2016) Erratum: [Phys. Lett. B **772**, 879 (2017)] arXiv:1606.02699 [hep-ex]